Fluorophore Coupling to Internal Modes of Bragg Gratings

Fluorophore Coupling to Internal Modes of Bragg Gratings

*Ramachandram Badugu[1], Jieying Mao[1], Douguo Zhang[2], Emiliano Descrovi[3,4], and Joseph R. Lakowicz[1]**

[1]Center for Fluorescence Spectroscopy, Department of Biochemistry and Molecular Biology, University of Maryland School of Medicine, 725 West Lombard Street, Baltimore, MD 21201, USA.

[2]Institute of Photonics, Department of Optics and Optical Engineering, University of Science and Technology of China, Hefei, Anhui, 230026, China

[3]Department of Applied Science and Technology, Polytechnic University of Turin, Corso Duca degli Abruzzi 24, 10129 Turin, Italy

[4]Department of Electronic Systems, Norwegian University of Science and Technology, O.S. Bragstads plass 2b, 7034 Trondheim, Norway

RECEIVED DATE (to be automatically inserted after your manuscript is accepted if required according to the journal that you are submitting your paper to)

TITLE RUNNING HEAD: Internal Mode Coupled Emission from Bragg Gratings

Corresponding author. E-mail: jlakowicz@som.umaryland.edu

CORRESPONDING AUTHOR FOOTNOTE (Word Style "FA_Corresponding_Author_Footnote"). Clarify all corresponding authors' addresses by accompanying footnotes if they are not apparent from the affiliation line. Telephone numbers, fax numbers, and e-mail addresses may all be included in the corresponding author footnotes. If an author's address is different than the one given in the affiliation line, this information may also be included here.

Abstract

Multi-layer structures with two dielectrics having different optical constants, and no structural features in the x-y plane, can display photonic band gaps (PBG) and are called one-dimensional photonic crystals (1DPC). If the top layer thickness is carefully selected the electromagnetic energy can be trapped at the top surface. These highly enhanced fields are called Bloch surface waves (BSWs). The BSW resonance angles are sensitive to the dielectric constant above the top dielectric layer. As a result, BSW structures have been used for surface plasmon resonances (SPR)-like measurements without the use of a metal film. However, the emphasis on surface localized BSWs has resulted in limited interests in fluorophore interactions with other optical modes of 1DPCs or Bragg gratings without the different thickness top layer. Herein, three different fluorescent probes were used to cover the short, center and long wavelengths of the PBG. We demonstrate efficient coupling of fluorophores to both the BSW and internal modes (IM) of a 1DPC. Coupling to the IM is expected to be low because of the micron-scale distances between the fluorophores and IM which exists inside the Bragg gratings. At different wavelengths or observation angles the internal mode-coupled emission (IMCE) can occur with the first three modes of the multi-layer. This coupling is not dependent on a BSW mode. IMCE was also observed for a monolayer of fluorophore-labeled protein. IMCE enables sensitive detection of surface bound fluorophores. Applications are anticipated in high sensitivity detection and super-resolution imaging.

Keywords: One-dimensional photonic crystals, Optical modes, Bloch surface waves, Bloch surface wave-coupled emission, Internal mode coupled emission, Bragg gratings.

Introduction

Detection of fluorophores on glass surfaces and slides has grown steadily during the past three decades. For example, the introduction of biomolecule-specific fluorophores stimulated the use of fluorescence microscopy for cell imaging.[1] This trend was further enhanced by confocal detection and/or multi-photon excitation which decreased out-of-focus emission and increased contrast.[2] There has also been rapid growth of fluorescence detection of surface-bound fluorophores for analytical applications such as immunoassays,[3] proteomics[4] and DNA sequencing.[5] All these applications use the free-space emission of biomolecules labeled with specific fluorophores. To avoid laborious labeling procedures and possible perturbations of the biomolecules by the fluorophores there is high interest in label-free methods. The most widely used label-free method is surface plasmon resonance (SPR) which uses glass slides with a thin layer of gold, about 40 nm thick, that displays intense absorption at a specific angle above the critical angle.[6] The SPR resonances display small angular shift which depends on the mass of a biomolecule binding to the surface and small changes in refractive index at the gold-water interface. Because these angular shifts are small, less than 1°, several methods have been described which increase the sensitivity of the SPR, such as phase sensitive detection,[7] substrates with gratings,[8] waveguides,[9] or metallic particles.[10]

During the past decade there has been rapid development of plasmonic substrates which use enhanced fluorescence to provide selective detection of surface-bound fluorophores. One of the earliest methods is surface plasmon-coupled emission (SPCE) wherein excited state fluorophores near the metal surface creates plasmons, which are detected at the plasmon resonance angle for the emission wavelength.[11,12] SPCE has been extended to include metal films coated with a single

dielectric layer to create metal-dielectric waveguides (MDW).[13] For SPCE and MDW structures the incident light is trapped at the top dielectric-air or water interface resulting in an enhanced excitation field. The emission at each wavelength is coupled through the substrate at a single angle from the normal z-axis, which provides selective detection of surface-bound fluorophores. Metallic surfaces have the disadvantage of quenching emission from fluorophores within 10 nm of the metal surface.[14,15] This quenching effect has been avoided by the use of all-dielectric BSW structures with photonic band gap (PBG) which trap light at the surface due to the high incident wavevector of the surface-bound electromagnetic waves. The trapped state is known as a Bloch surface wave (BSW),[16] which should not be confused with Bloch waves which exist within any periodic structure.[17] In the present report we refer to Bloch waves as internal modes (IM) of the structure. We consider only one-dimensional photonic crystals (1DPC) which have multiple planar films with different refractive indices. If the top dielectric layer has a different and suitable thickness the incident light can be trapped at the top layer.[18,19] 1DPC structures which contain only transparent optical materials and have low optical losses. As a result, the BSW resonances show a very narrow angular distributions and a corresponding strong field enhancement at the surface.[20,21] The BSW resonance angle is sensitive to the dielectric constant above the structure which permits label-free SPR-like detection of surface binding.[22] Similar to surface plasmons, the BSWs have an evanescent field which penetrates a short distance into the sample. This evanescent field has been used for enhanced excitation of surface-bound fluorophores. The excited state fluorophores can couple with the BSW field and radiate through the substrate over a narrow range of wavelengths and angles.[23,24] This phenomenon is called Bloch surface wave-coupled emission (BWCE).

SPR, SPCE and BWCE all depend on evanescent fields which have short penetration lengths into the sample. As a result of the need for evanescent wave-sample interactions, research has

focused on fluorophore coupling to the surface modes.[13,25] However, 1DPCs also display internal modes (IM) wherein the optical field is localized within the multilayer structure. Because the IMs have shorter evanescent tails penetrating into the sample, they have been ignored for detection of surface-bound fluorophores. Stated otherwise, fluorophores coupling to IM modes is generally thought to be weak because the fluorophores are hundreds of nanometers or several microns away from the locations where most of the IM mode energy is confined. Fluorophore coupling to IM modes has been detected in previous angle-dependent measurements of the coupled emission.[21] Internal mode-coupled emission (IMCE) has also been observed using back focal plane (BFP) imaging of reflected light or coupled emission.[26,27] However, because of the emphasis on the surface modes coupling, the emission coupling to IM modes has rarely been examined and usefulness of IMCE has not yet been recognized.

In the present report we characterize the properties of IMCE. The IMCE intensities are comparable to BSW-coupled emission intensity but occur at different angles and wavelengths through the substrate. IMCE does not require the presence of a BSW and can be used with any Bragg grating (BG). We show the IMCE intensity depends on the reflectivity spectrum of the BG. The internal modes are almost completely inside the 1DPC or BG, and the coupling angles are almost independent of the refractive index above the structure, which makes IMCE convenient for detection of surface-bound fluorophores in aqueous solution without concern for a specific top layer thickness or change in the coupling angle. The BG and 1DPC multi-layer structures have no nanoscale features in the x-y plane, can be fabricated by vapor deposition[28] and therefore available for large area samples at low cost. They can be made with any dielectric and designed for use over a wide range of wavelengths from the UV to the NIR. 1DPCs can also be fabricated by spin coating of polymers[29] inorganic sol gels,[30] or with a small contrast ratio between the two dielectric

materials.[31] These properties of 1DPCs will enable the use of IMCE in a wide range of bioaffinity assays, spotted array applications, and potentially point-of-care devices.

Materials and Methods

The fluorescent probes rhodamine 6G (Rh6G) and Nile Blue (NB) were obtained from Invitrogen, Inc. [Ru(bpy)$_2$ dppz](PF$_6$), where bpy is 2,2'bipyridine, dppz is dipyridophenazine and PF$_6$ is hexafluorophosphate, was obtained from Sigma-Aldrich and hereafter called Ru(dppz). All probes were used without further purification. The molecular structure and emission spectra of these probes in PVA were shown in Figure 1. These probes were selected to overlap with or be close to the PBG of the 1DPC. Each probe was dissolved in 1% poly-vinylalcohol (PVA) in water and spin coated on glass slides on the 1DPC, using conditions described previously to obtain a 45 nm thick layer of PVA.[21] Rhodamine B-labeled streptavidin (RhB-SA) was obtained from Invitrogen, Inc. A monolayer of RhB-SA, with a thickness near 4 nm, was obtained by covering the 1DPC with a 1 mg/ml solution in pH 7.2 phosphate buffer for 30 min at 4 °C, followed by rinsing with the same buffer without SA.

The 1DPC was made by plasma-enhanced chemical vapor deposition (PECVD) of silica (SiO$_2$) and silicon nitride (Si$_3$N$_4$) on standard microscope slides. This structure consisted of alternating layers of the low (L) and high (H) refractive index (n) dielectrics (Figure 2B). The top layer of the low-refractive index SiO$_2$ was a different thickness needed to support a Bloch surface wave (BSW) at wavelengths near 580 nm but this thickness does not support BSW at wavelengths above 650 nm.[21] Simulated reflectance were obtained using TFCalc.[32] Simulations of dipole emission or incident fields were calculated using software from Lumerical, Inc.[33] and confirmed by a code based on the algorithm used in reference 34. The low (L) refractive index of SiO$_2$ was used with a

null imaginary part. The high (H) refractive index of Si_3N_4 ranged from $n_H = 2.196 + i0.033$ at 550 nm to $n_H = 2.144 + i0.016$ at 633 nm.[21] The imaginary component resulted in a finite angular width which facilitated some of the simulations.

The experimental geometry is moderately complex, and to avoid ambiguity is shown in detail (Figure 2A). The 1DPC is mounted on a hemicylindrical prism and optically coupled with index matching fluid (glycerol) to avoid total internal reflection (TIR) from the glass slide.[35] The prism allows light above the glass-air critical angle to enter and create an evanescent field at the top SiO_2-PVA layer. The prism also allows the coupled emission above the critical angle to be measured in the far-field. The z-axis is the laboratory vertical axis and is along the long axis of the prism. The incident light for excitation can be through the prism, known as the Kretschmann (KR) configuration, or directly from the air side of the sample known as the reverse Kretschmann (RK) configuration. The terms KR and RK usually refer to the incident light, but we use these same terms to describe the emission. In this report the excitation was always in the RK configuration from the air side, at 180E. Similar results were obtained for KR excitation (not shown). Emission is measured on the prism side (KR) from 0E to 80E, and from the air side (RK) from 95E to 140E. The RK emission is also described as free-space emission. The prism has a diameter of 1 inch and the end of the observation fiber, with a diameter of 1.0 mm, is placed 2 cm away from the prism surface or about 2.5 cm from the illuminated spot. Most of the measurements are S-polarized meaning the excitation and emission polarizer are aligned with the vertical z-axis and parallel with the surface of the 1DPC. For P-polarized emission measurements, the excitation polarizer remains aligned with the z-axis but the emission polarizer is tilted perpendicular to the z-axis. In some cases, the incident light was along the y-axis, but the S-coupled emission was nearly the same as with incident light polarized along the z-axis. A long-pass filter is used to remove reflected or

scattered incident light. The emission passing through the fiber is measured with either an Ocean Optic SD2000 spectrofluorometer or a Pico Quant MicroTime 300 spectrofluorometer.

Results and Discussion

Simulated optical properties of the 1DPC. In previous publications we reported coupled emission from photonic and plasmonic structures. For thin metallic films the coupled emission occurred at the surface plasmon resonance angle,[11,12] and for dielectric photonic structures the coupled emission occurred at the wavelength and angle of the BSW resonance.[21] Coupled emission with the photonic structure at angles larger than the BSW angles were noted but not discussed.[21] The fluorophore in Figure 1 were selected because the emission spectra of Rh6G, NB and Ru(dppz) overlap with the resonances of the 1DPC. The simulated reflectance spectra show strong narrow S-polarized dips in reflectivity which depend on the incident wavelength (Figure 3). The sharp resonances at the shorter wavelengths are due to the S-polarized BSW modes. Wider but less pronounced dips in the reflectivity are seen at longer wavelengths, which are shown below to be due to internal modes (IM) of the 1DPC. By design, the present 1DPC does not display a BSW mode above 650 nm to allow us to determine if the BSW mode contributed to internal mode-coupled emission.

The optical modes of the 1DPC can be observed by the angle-dependent reflectivity at a single wavelength (Figure 3B). The BSW modes are seen as sharp resonances near 45°, and the IM appears at larger observation angles. These results show BSW modes for 555 and 600 nm, but BSW modes are essentially absent at 675 nm. The IM modes are still present for 675 nm and would be present without the thicker top layer of SiO_2 (not shown). The IM modes are very robust and exist even if the spaces above the 1DPC is all water (n = 1.33). In contrast, the BSW mode is not

present when the 1DPC in Figure 2B is covered with water. A different 1DPC structure is needed to support a BSW mode in water.

The optical modes (BSW or IM) associated with the dips in reflectivity (Figure 3) were assigned by simulations of the field intensity ($|E|^2$) distributions in the 1DPC for illumination at the resonance wavelengths and angles. At 580 nm with S-polarized incident light at 44.1° the intensity is strongly localized at the surface of the 1DPC and enhanced 1400-fold (Figure 4A), which is characteristic of a BSW mode.[36,37] The optical field is localized by two effects. Light cannot escape from the top due to total internal reflection. Light propagation through the bottom is restricted by the PBG and can only escape by tunneling. The electric field distribution with 580 nm incident light changes for different angles of illumination. The first internal mode (IM1) for illumination at 57.8E is inside the 1DPC and has a maximum intensity in the center of the 1DPC with a symmetrical intensity distribution (Figure 4B). The second and third internal modes (IM2 and IM3) for illumination at 68.2Eand 85, respectively, have more complicated intensity distribution (Figures 4C and 4D). Similar results were obtained at 600 nm where the BSW field was enhanced nearly 900-fold (Figure S1). At 675 nm the 1DPC showed similar shaped internal IM1 and IM2 modes (Figure S2). At 675 nm the BSW mode is shifted close to the critical angle and there was only a 4-fold field enhancement of the BSW mode at 675 nm at the 1DPC surface, which is comparable to TIR.[35] This is in contrast to the apparent BSW mode at shorter wavelengths where BSW field intensities are greatly enhanced at 580 and 600 nm. The difference between a TIR and BSW mode can be seen in Figure S2(A) where the TIR starts abruptly at the PVA-air interface and the BSW mode is localized in both the PVA and air space. The IM field intensities at the surface for 675 nm are comparable to or lower than those found for TIR. BSW-coupled emission at 675

nm is not expected because the BSW mode is no longer significant (Figure S2). For all three wavelengths the maximum intensity location of IM1 is about 1000 nm from the surface and not within the near-field of the excited state fluorophores. The most intense region of the IM2 mode is about 500 nm from the surface. Fluorophore coupling is expected to be very weak at these long distances. Coupling between two fluorophores for fluorescence resonance energy transfer (FRET) occurs at distances no greater than 8 nm[38] and FRET between fluorophores and a continuous layer of gold may occur to about 16 nm.[14,39] Coupled emission via the internal modes is expected to be weak at any wavelength or angles because they have very small amplitudes at the top surface where the fluorophores are localized and are too distant from the IM modes for FRET-type near-field interactions.

Coupled emission spectra for Rh6G. The coupled emission of Rh6G is highly modified when placed on the 1DPC (Figure 5). On a plain glass slide, the emission spectrum (dashed lines in Figure 5) is not significantly dependent on observation angle. On the 1DPC the apparent emission spectra become very narrow and confined to a small range of wavelengths which do not appear to follow the free-space emission spectra. The coupled emission shifts to shorter wavelengths as the observation angle is increased in the BSW range, 41E to 47E (Figure 5A). At larger angles from 50E to 70E, the emission maxima are coupled to the first internal mode and also shift to shorter emission maxima at larger observation angles (Figure 5B). The coupled emission maxima are strongly dependent upon the observation angle and confined to a small range of angles (Figure 6A). On the other hand, P-polarized emission was insensitive to the observation angle (Figure S3).

When we first observed these spectral shifts we thought the emission spectra were red-shifted at larger angles. A similar effect was observed for a number of different fluorophores. We later

realized that the BSW-coupled modes occurred from 41E to 47E, and that new modes appeared at larger angles for 50E to 70E, which we now assign to IM-coupled emission. We were hesitant to reach this conclusion because the peak intensity envelope of the first internal mode (IM1) coupled-emission was only about 10-fold less than the BSW-coupled emission. These relative intensities are very different from the 1000-fold enhanced intensities of the BSW modes and the 4-fold enhancements of the IM1 mode at surface with light incident at the resonance value for each wavelength. However, the difference in emission intensities could not be due to an amplified excitation field because the experiments were performed with RK excitation at 180E and emission S-polarized along the z-axis (Figure 2A). Because of the RK mode of excitation the relative intensities reflect the coupling efficiency to the BSW or IM1 modes. The connection of the observed maxima with each mode can be clarified by plotting the normalized intensities (Figure 5C). The relativity high intensities of the IMCE (Figure 5B) suggest that it could be useful for surface-selective detection.

Coupled emission of Nile Blue. We were surprised by the relatively high intensity of the IM1-coupled emission from Rh6G, and questioned if the absence of a BSW mode facilitated coupling to the IM1 intensity. To clarify this question, we selected the probe Nile Blue (NB). NB has longer emission wavelength over 650 nm (Figure 7), where the BSW mode is no longer significant (Figure S2). The 660 nm emission maximum of NB is much longer than the emission maxima of Rh6G at 550 nm. BWCE was not observed for NB on the 1DPC, presumably because the BSW mode is weak or non-existent at this wavelength. The emission is still strongly directional (Figure 7C) but the combination of observation angle and wavelength is consistent with coupling to the IM1 and IM2 modes (shown below). As before the P-polarized emission spectra were mostly the same at

all observation angles (Figure S4). Accordingly, at 660 nm the 1DPC in Figure 2B is no longer sustaining a BSW mode and present results suggest that IMCE can be observed with any Bragg grating without a BSW mode.

Coupled emission with Ru(dppz). Coupling of NB with the IM1 and IM2 modes, at wavelengths larger than the BSW, suggested the BSW modes are not necessary for coupling to the IM modes. The absence of a BSW pathway may increase coupling to the IM modes. To further demonstrate coupled emission to the IM modes we examined a metal-ligand complex (MLC) Ru(dppz) with a wide emission spectrum ranging from 540 to 800 nm (Figure 8, dashed lines). Because of the width of the Ru(dppz) emission the angle-dependent spectra were expected to contained contributions of coupled emission from more than one mode. We reasoned that detection of both BSW and IM-coupled emission from a single fluorophore would reveal the relative efficiency of BSW and IM coupling. At observation angles of 41E to 46E coupled emission is observed from both the BSW and IM1 modes, but in different emission wavelength ranges. This result is consistent with the NB results which showed IM1 coupled emission near 675 nm (Figure 7). Once again the P-polarized emission spectra did not show consistent angle-dependent shifts (Figure S5). The IM1 intensity is about 5-fold less than the BSW intensity (Figure 8A). These results confirm that IMCE provides high coupled emission intensities with RK incident light, without the high surface field enhancements with KR incident light. A similar argument can be made by comparison of the IM1 versus IM2 relative intensities (Figure 8B). The connections between the wavelength-dependent emission maximum and the optical modes can be seen in the normalized intensities (Figure 8C), where some emission is even seen with the IM3 mode.

Free-space emission intensities. The coupled emission of Ru(dppz) is confined to a very narrow range of angles, and contributions from the BSW, IM1 and IM2 modes can be resolved by the

smaller peaks at higher angles (Figure 6B). If the BSW mode was not present the smaller peaks would be dominant. We noticed that the free-space emission within Ru(dppz) was very low, as was the free-space intensity of Rh6G (Figure 6). In contrast the free-space emission of NB was high (Figure 7C). These results are consistent with the observed coupling of Rh6G to the BSW mode, and Ru(dppz) coupling with the BSW, IM1 and IM2 modes, resulting in their low free-space intensities. In contrast, NB could not couple with a BSW mode and could only couple to the IM1 and IM2 modes. As a result, the free-space emission from NB is higher than the other two fluorophores.

Dispersion diagrams and mode coupling. The dispersion diagram for the 1DPC in Figure 9 shows the angle and wavelength-dependent properties of the structure. Superimposed on this diagram are the angle-dependent maxima for the three fluorophores studied. The agreement between the simulations and experimental data is not perfect which is probably is the result of the actual 1DPC having slightly different dimensions and/or optical properties than the simulated 1DPC. However, it is clear that the apparent emission maxima of the three different fluorophores on the 1DPC are correlated with the listed modes. The IM1 modes can be observed at the same angles as the BSW mode. Because its long emission spectrum, NB only couples to IM1 and IM2, whereas Rh6G couples to BSW, IM1 and IM2 and due to its wide emission spectrum Ru(dppz) couples to four modes, BSW and IM1, IM2 and IM3. The striking feature of Figure 9 is that the angle-dependent emission maxima are independent of fluorophore, and a characteristic of the optical modes of the 1DPC. More specifically, the same emission maximum is observed for any fluorophores on the 1DPC or Bragg structure when measured at the same observation angle. Another important result is that fluorophores can couple with any optical mode in the 1DPC if

there is spectral and angular overlap. This property is similar to FRET which occurs with any donor-acceptor pair and depends only on spectral overlap.[38]

Sensitivity of IMCE. To demonstrate the use of IMCE to measure low intensity fluorescence we examined the 1DPC coated with a single monolayer of rhodamine B-labeled streptavidin (RhB-SA). The effective probe concentration for the monolayer is many-fold lower than the previous measurements with labeled PVA layers. The BSW-coupled emission was found to be at least 10-fold more intense than the free-space emission measured in the RK-direction. The IMCE intensity is about 2-fold larger than the free-space intensity (Figures 10 and S6). Thus, IMCE is not as sensitive as BWCE but the intensity is comparable to or larger than the free-space emission. The emission spectra of RhB-SA displayed the same dependence on observation angle for the BSW and IM modes (Figure 10). The angle-dependent emission maxima follow the dispersion diagram shown in Figure 9 (data not shown). These results suggest IMCE can be used for a wide range of surface-bound bioassays.

The emphasis of this paper is to demonstrate that coupled emission can be observed with a Bragg grating, independent of the presence of a BSW surface mode. The use of a Bragg grating is in contrast to the use of BSW structure for sensing, as seen by their use as a substitute for SPR[40,41] and fluorescence detection of surface-bound fluorophores.[42,43] A common feature of these BSW applications is on the use of localized surface-waves and interactions with the sample. As discussed above, BSW are not present on all multilayer structures and a change in the sample solution can eliminate the BSW resonance in the sample. The present paper attempts to overcome this narrow vision of sensing with multi-layer BSW structures and to expand their use by coupling to internal modes using Bragg structures. These IM modes are very robust and weakly, if affected at all, by the sample dielectric constant. Our results show that excited state fluorophores can couple with

the IM modes over micron distances and display strongly directional emission. Importantly the intensities of the IM coupled emission can be comparable to those of BSW coupled emission.

Conclusions

This paper agrees with the results from an earlier report,[23] which reported strong modification of the emission spectra of a rhodamine dye on a BSW structure. The rhodamine spectrum change is from a typical single wide emission on glass to two narrow emission spectra on a BSW structure. While not certain, it seems likely that the spectral redistribution reported was separate coupling to a BSW and an IM mode.[23] This not a criticism of the authors, but merely an alternative explanation for their results.

Another potential use of IMCE is for detection of super-critical angle fluorescence (SCF), which occurs at angles above the critical angle.[44] This emission can be collected using parabolic reflective detectors.[45] SCF has already been used without a BSW structure or Bragg grating for high sensitivity immunoassays without wash steps[46] and detection of single nucleotide polymorphisms without a microscope objective.[47] In the case of fluorescence microscopy, SCF contains high wavevector components which increases spatial resolution to provide sub-diffraction limited spatial resolution.[48-50] The SCF results were obtained without Bragg grating. The use of Bragg grating substrates may provide a method to suppress the lower wavevector components which decrease spatial resolution.

In summary, a simple multi-layer Bragg grating structure can couple the emission of near-surface fluorophores into IM modes at different angles and wavelengths can be easily fabricated without the delicate structural design to obtain a BSW resonance. These structures are also widely

available from optic companies. IMCE can have an impact in development of new clinical sensing instruments and point-of-care devices.

Acknowledgments: R. Badugu, J. Mao and J. R. Lakowicz thank the National Institute of Gneral Medical Sciences for support under R01 GM125976 and R21 GM129561. D. Zhang acknowledges support from the National Nature Science Foundation of China (No. 61427818 and No. 11774330), the Ministry of Science and Technology of China (No. 2016UFA0200601), the Anhui Initiative in Quantum Information Technologies, (No. 1608085102), Anhui Provincial Science and Technology Major Projects (No. 18030901005), the Fundamental Research Funds for Central Universities (No WK2340000084), the Foundation of Key Laboratory of Environmental Optics and Technology (No. 2005DP173065-2091-XX), and Longshan Academic Research Program of SWUST (No. 17LZX626). D.G.Z. is also supported by USTC Scholarship. E. Descrovi acknowledges support from the Italian Flagship Project NANOMAX (Progetto Randiera MIUR PNR 2011-2013) and the EU FP7 project BILPBA (No. 318035).

References

1. Johnson, I., and Spence, M. T. Z. (Eds). (2010). *The Molecular Probes Handbook. 11th Ed.*, Life Technologies Corp.
2. Mondal, P. P. And Diaspro, A. (Eds). (2015). *Fundamentals of Fluorescence Microscopy*, Springer, New York, 218 pp.
3. Vashist, S. K., and Luong, J. H. T. (Eds). (2018). *Handbook of Immunoassay Technologies: Approaches, Performances, and Applications*, 1st Ed. Academic Press, 496 pp.
4. Twyman, R. (2013). *Principles of Proteomics*, 2nd Ed. Garland Science, 260 pp.

5. Low, L. And Tammi, M. (Eds). (2017). *Bioinformatics: A Practical Handbook of Next Generation Sequencing and its Applications,* World Scientific Publishing Co. 252 pp.
6. Hinman, S. S., McKeating, K. S., and Cheng, Q. (2018). Surface plasmon resonance: material and interface design for universal accessibility, *Anal. Chem.,* 90:19-39.
7. Naraoka, R., and Kajikawa, K. (2005). Phase detection of surface plasmon resonance using rotating analyzer method, *Sensors and Actuators B.,* 107:952-956.
8. Daghestani, H. N., and Day, B. W. (2010). Theory and applications of surface plasmon resonance, resonant mirror, resonant waveguide grating, and dual polarization interferometry biosensors, *Sensors*, 10:9630-9646.
9. Alleyne, C. J., Kirk, A. G., MCPhedran, R. C., Nicorovici, N. P., and Maystre, D. (2007). Enhanced SPR sensitivity using periodic metallic structures, *Optics Express*, 15:8163-8169.
10. Juve, V., Cardinal, M. F., Lombardi, A., Crut, A., Maioli, P., Perez-Juste, J., Liz-Marzan, L. M., Del Fatti, N., and Vallee, F. (2000). Size-dependant surface plasmon resonance broadening in nonspherical nanoparticles: Single gold nanorods, *Nano Letts.,* 13:2234-2240.
11. Lakowicz, J. R. (2004). Radiative decay engineering 3. Surface plasmon-coupled directional emission, *Anal. Biochem.,* 324:153-169.
12. Gryczynski, I., Malicka, J., Gryczynski, Z., and Lakowicz, J. R. (2004). Radiative decay engineering 4. Experimental studies of surface plasmon-coupled directional emission, *Anal. Biochem.,* 324:170-182.
13. Badugu, R., Szmacinski, H., Ray, k., Descrovi, E., Ricciardi, S., Zhang, D., Chen, J., Huo, Y., and Lakowicz, J. R.(2015). Fluorescence spectroscopy with metal-dielectric waveguides, *J. Phys. Chem. C.,* 119:16245-16255.
14. Reineck, P., Gomez, D., Ng, S. H., Karg, M., Bell, T., Mulvaney, P., and Bach, U. (2013). Distance and wavelength dependent quenching of molecular fluorescence by Au@SiO_2 core-shell nanoparticles, *ACS Nano*, 7:6636-6648.

15. Ray, K., Szmacinski, H., Enderlein, J., and Lakowicz, J. R. (2007). Distance dependence of surface plasmon-coupled emission observed using Langmuir-Blodgett films, *Appl. Phys. Letts.,* 90:251116-1/3.
16. Rames-Mendieta, F., Halevi, P. (1999). Surface electromagnetic waves in two-dimensional photonic crystals: effect of the position of the surface plane, *Phys. Rev. B.,* 59:15112-15120.
17. Saleh, B. E. A., and Teich, M. C. (Eds.) (2007). *Fundamentals of Photonics*, 2nd Ed. Wiley, 1177 pp.
18. Robertson, W. M. (1999). Experimental measurement of the effect of termination on surface electromagnetic waves in one-dimensional photonic bandgap arrays, *J. Light. Tech*., 17:2013-2017.
19. Ballarini, M., Frascella, F., Enrico, E., Mandracci, P., De Leo, N., Michelotti, F., Giorgis, F., Descrovi, E. (2012). Bloch surface waves-controlled fluorescence emission: Coupling into nanometer-sized polymeric waveguides. *Appl. Phys. Lett*., 100:063305.
20. Toma, K., Descrovi, E., Toma, M., Ballarini, M., Mandracci, P., Giorgis, F., Mateescu, A., Jonas, U. Knoww, W., and Dostalek, J. (2013). Bloch surface wave-enhanced fluorescence biosensor, *Biosen. Bioelec*., 43:108-114.
21. Badugu, R., Nowaczyk, K., Descrovi, E., and Lakowicz, J. R. (2013). Radiative decay engineering 6: Fluorescence on one-dimensional photonic crystals, *Anal. Biochem.,* 442:83-96.
22. Sinibaldi, A., Occhicone, A., Munzert, P. Danz, N., Sonntag, F., Michelotti, F. (2018). Label-Free Monitoring of Human IgG/Anti-IgG Recognition Using Bloch Surface Waves on 1D Photonic Crystals, *Biosensors,* 8:71.
23. Liscidini, M., Galli, M., Shi, M., Dacarro, G., Patrini, M., Bajoni, D., Sipe, J.E. (2009). Strong modification of light emission from a dye monolayer via Bloch surface waves, *Opt. Lett.* 34:2318-2320.
24. Sepe, E., Sinibaldi, A., Danz, N., Munzert, P., Michelotti, F. (2019). Anisotropic Fluorescence Emission and Photobleaching at the Surface of One-Dimensional Photonic Crystals Sustaining Bloch Surface Waves. II. Experiments, *J. Phys. Chem, C* 123:21176-21184.

25. Badugu, R., Mao, J., Blair, S., Zhang, D., Descrovi, E., Angelini, A., Huo, Y., and Lakowicz, J. R. (2016). Bloch surface wave-coupled emission at ultraviolet wavelengths, *J. Phys. Chem. C.,* 120:28727-28734.

26. Zhang, D., Badugu, R., Chen, Y. Yu, S., Yao, P., Wang, P., Ming, H., and Lakowicz, J. R. (2014). Back focal plane imaging of directional emission from dye molecules coupled to one-dimensional photonic crystals, *Nanotech*., 25:145202-1/10.

27. Han, L., Zhang, D., Chen, Y., Wang, R., Zhu, L., Wang, P., Ming, H., Badugu, R., and Lakowicz, J. R. (2014). Polymer loaded propagating modes on a one-dimensional photonic crystal, *Appl. Phys. Letts.,* 104:061115-1/5.

28. Smith, D. (1995). *Thin-Film Deposition: Principles and Practices,* 1st ed. McGraw-Hill Ed., 616 pp.

29. Menon, V. M., Luberto, M., Valappil, N. V., and Chatterjee, S. (2008). Lasing from InGaP quantum dots in a spin-coated flexible microcavity, *Optics Exp.,* 16:19535-19537.

30. Inouye, H., Arakawa, M., Ye, J. Y., Hattori, T., Nakatsuka, H., and Hirao, K. (2002). Optical properties of a total-reflection-type one-dimensional photonic crystal, *J. Quantum Elec*., 38:867-871.

31. Wei, L., Zhang, X. Z., Wang, Z. H., Wu, Q., Liu, L. C., Xu, J. J., and Tang, B. Q. (2010). Observation of modulated spontaneous emission of rhodamine 6G in low refractive index contrast 1D-periodic gelatin film, *Science China*, 53:54-58.

32. TFCalc, LighTec GMBH, Munich, Germany.

33. Lumerical Solutions, Inc., Vancouver, BC, Canada.

34. Polerecký, L., Hamrle, J., MacCraith, B. D. (2000). Theory of the radiation of dipoles placed within a multilayer system, *Appl. Opt.* 39:3968-3977.

35. Axelrod, D., Burghardt, T. P., and Thompson, N. L. (1984). Total internal reflection fluorescence, *Biophys. Bioeng.,* 13:247-268.

36. Robertson, W. M., and May, M. S. (1999). Surface electromagnetic wave excitation on one-dimensional photonic band-gap arrays, *Appl. Phys. Letts.,* 74:1800-1802.

37. Aurelio, D., and Liscidini, M. (2017). Electromagnetic field enhancement in Bloch surface waves, *Phys. Rev. B.,* 96:045308-1/7.

38. Lakowicz, J. R. (2006). *Principles of Fluorescence Spectroscopy, 3rd ed.,* Springer, New York, 954 pp.

39. Zhang, X., Marocico, C. A., Lunz, M., Gerard, V. A., Gun-ko, Y. K., Lesnyak, V., Gaponik, N., Susha, A. S., Rogach, A. L., and Bradley, A. L. (2012). Wavelength concentration, and distance dependence of nonradiative energy transfer to a plane of gold nanoparticles, *ACS Nano*, 6:9283-9290.

40. Farmer, A., Friedli, A. C., Wright, S. M., and Robertson, W. M. (2012). Biosensing using surface electromagnetic waves in photonic band gap multilayers, *Sensors Actuators B.,* 173:79-84.

41. Khan, M. U., and Corbett, B. (2016). Bloch surface wave structures for high sensitivity detection and compact waveguiding, *Sci. Tech. Adv. Mat.,* 17:398-409.

42. Rizzo, R., Alvaro, M., Danz, N., Napione, L., Descrovi, E., Schmieder, S., Sinibaldi, A., Chandrawati, R., Rana, S., Munzert, P., Schubert, T., Maillart, E., Anopchenko, A., Rivolo, P., Mascioletti, A., Sonntag, F., Stevens, M.M., Bussolino, F., Michelotti, F. (2018). Bloch surface wave label-free and fluorescence platform for the detection of VEGF biomarker in biological matrices, *Sensors Actuators B.,* 255:2143-2150.

43. Sinibaldi, A., Doricchi, A., Pileri, T., Allegretti, M., Danz, N., Munzert, P., Giordani, E., Giacomini, P., Michelotti, F. (2020). Bioassay engineering: a combined label-free and fluorescence approach to optimize HER2 detection in complex biological media. *Anal. Bioanal. Chem.,* 412:3509–3517.

44. Luan, L., Sievert, P. R., Watkins, B., Mu, W., Hong, Z., and Ketterson, J. B. (2006). Angular radiation pattern of electric dipoles embedded in a thin film in the vicinity of a dielectric half space, *Appl. Phys. Letts.,* 89:031119-1/3.

45. Valimaki, H., and Tappura, K. (2009). A novel platform for highly surface-sensitive fluorescent measurements applying simultaneous total internal reflection excitation and super critical angle detection, *Chem. Phys. Letts.,* 473:358-362.

46. Ruckstuhl, T., Winterflood, C. M., and Seeger, S. (2011). Supercritical angle fluorescence immunoassay platform, *Anal. Chem.,* 83:2345-2350.

47. Krieg, A., Laib, S., Ruckstuhl, T., and Seeger, S. (2000). Fast detection of single nucleotide polymophisms (SNPs) by primer elongation with monitoring of supercritical angle fluorescence, *ChemBioChem*., 5:1680-1685.

48. Chazot, C. A. C., Nagelberg, S., Rowlands, C. J., Scherer, M. R. J., Coropceanu, I., Broderick, K., Kim, Y., Bawendi, M. G., So, P. T. C., and Kolle, M. (2020). Luminescent surfaces with tailored angular emission for compact dark-field imaging devices, *Nature Phtonics*, 1-6.

49. Kuang, C., Li, S., Liu, W., Hao, X., Gu, Z., Wang, Y., Ge, J., Li, H., and Liu, X. (2013). Breaking the diffraction barrier using fluorescence emission difference microscopy, *Scien. Reports*, 3:1441-1/6.

50. Winterflood, C. M., Ruckstuhl, T., Verdes, D., and Seeger, S. (2010). Nanometer axial resolution by three-dimensional supercritical angle fluorescence microscopy, *Phys. Rev. Letts.,* 105:108103-1/4.

Figure Legends:

Figure 1. Chemical structures of the probes and emission spectra in PVA on glass used in the present report.

Figure 2. (A), Optical geometry for emission measurements with a 1DPC using RK excitation. Incident wavelength is 470 nm for Rh6G and Ru(dppz) and 635 nm is for Nile Blue. (B), Dimensions and optical properties of the 1DPC. The far-field optical properties for 580, 600 and 675 nm incident wavelengths are shown in Figures 4, S1 and S2, respectively.

Figure 3. (A) Wavelength and (B) angle-dependent reflectivity spectra of the 1DPC. The numbers refer to the incident angle (A) or incident wavelength (B).

Figure 4. Field intensity ($|E|^2$) distribution for 580 nm incident light. (A) BSW resonance at 44.1 deg, (B) IM1 at 57.8 deg, (C) IM2 at 68.2 deg and (D) IM3 at 85.0 deg . Both S- and P-polarizations are shown.

Figure 5. Rh6G, S-polarized emission in the BSW range (A), and in the IM1 range (B). Dashed lines show the intensity normalized Rh6G emission spectrum from glass, which is insensitive to the observation angle. Panel C shows the normalized Rh6G, S-polarized emission in the BSW range and in the ranges for IM1 and IM2. Some selected angles are listed in the panel.

Figure 6. (A), Rh6G and (B) $Ru(bpy)_2(dppz)(PF_6)_2$ angular emission intensity distribution from the 1DPC. RK illumination using 470 nm at 180 degrees.

Figure 7. Nile Blue, S-polarized emission in the IM1 range (A), and in the IM2 range (B). Dashed lines show the intensity normalized Nile Blue emission spectrum from glass, which is insensitive to the observation angle. Note the wavelength axis is different from that used in Figure 5. Panel C shows the Nile Blue emission intensity distribution from 1DPC. RK illumination polarized along the Y-axis using 635 nm at 180 degrees.

Figure 8. BSW, IM1 and IM2-coupled emission from $Ru(bpy)_2(dppz)(PF_6)_2$ on 1DPC. Dashed lines show the intensity normalized ruthenium complex emission spectrum from glass λex = 470 nm. Panel C shows the corresponding normalized emission in the BSW, IM1, IM2 and IM3 ranges. Some selected angles are labeled in the panel.

Figure 9. Dispersion diagram for the 1DPC. The figure shows the reflectivity for a range of wavelengths and incidence angles. The dots represent the angle-dependent emission maxima and respective angles.

Figure 10. S-polarized emission from a monolayer of RhB-SA on 1DPC in the BSW range, and in the IM1 range. Normalized spectra are shown in the right panel. Only few selected spectra are labeled for clarity.

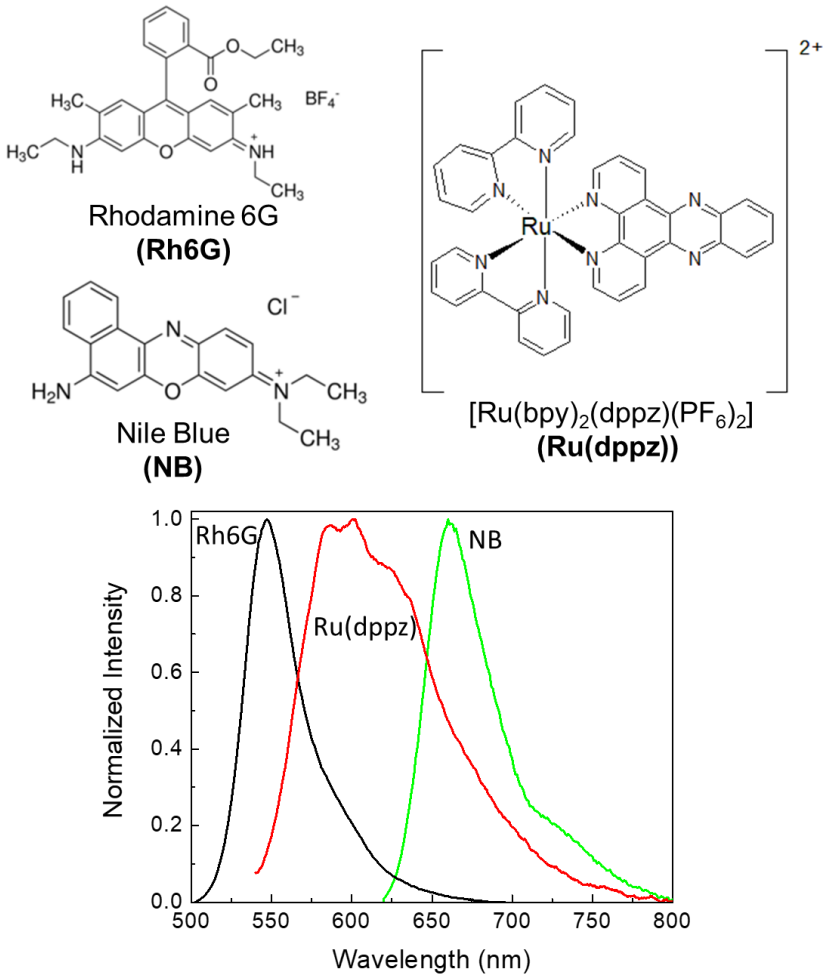

Figure 1. Chemical structures of the probes and emission spectra in PVA on glass used in the present report.

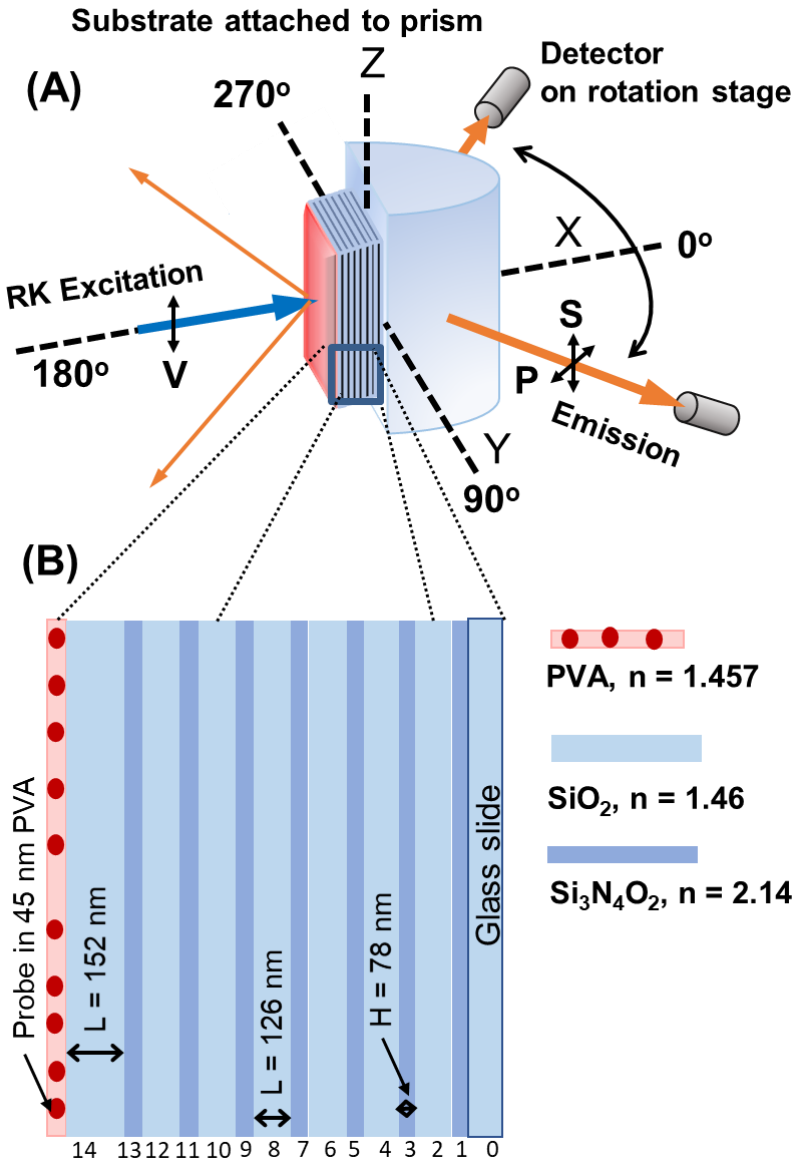

Figure 2. (A), Optical geometry for emission measurements with a 1DPC using RK excitation. Incident wavelength is 470 nm for Rh6G and Ru(dppz) and 635 nm is for Nile Blue. (B), Dimensions and optical properties of the 1DPC. The far-field optical properties for 580, 600 and 675 nm incident wavelengths are shown in Figures 4, S1 and S2, respectively.

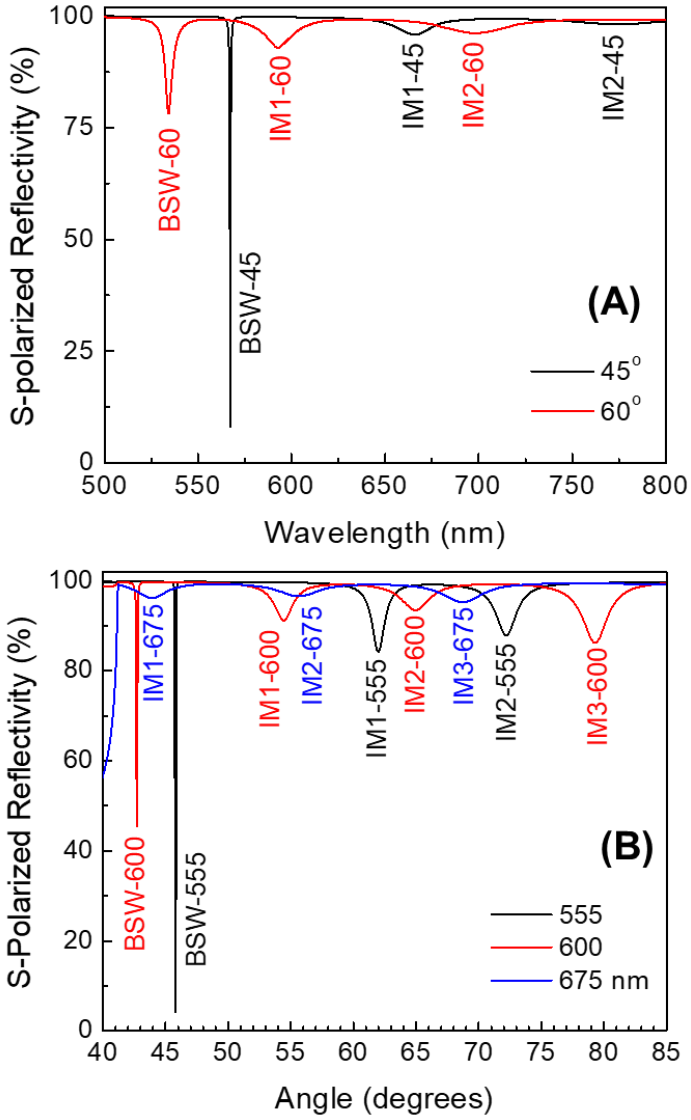

Figure 3. (A) Wavelength and (B) angle-dependent reflectivity spectra of the 1DPC. The numbers refer to the incident angle (A) or incident wavelength (B).

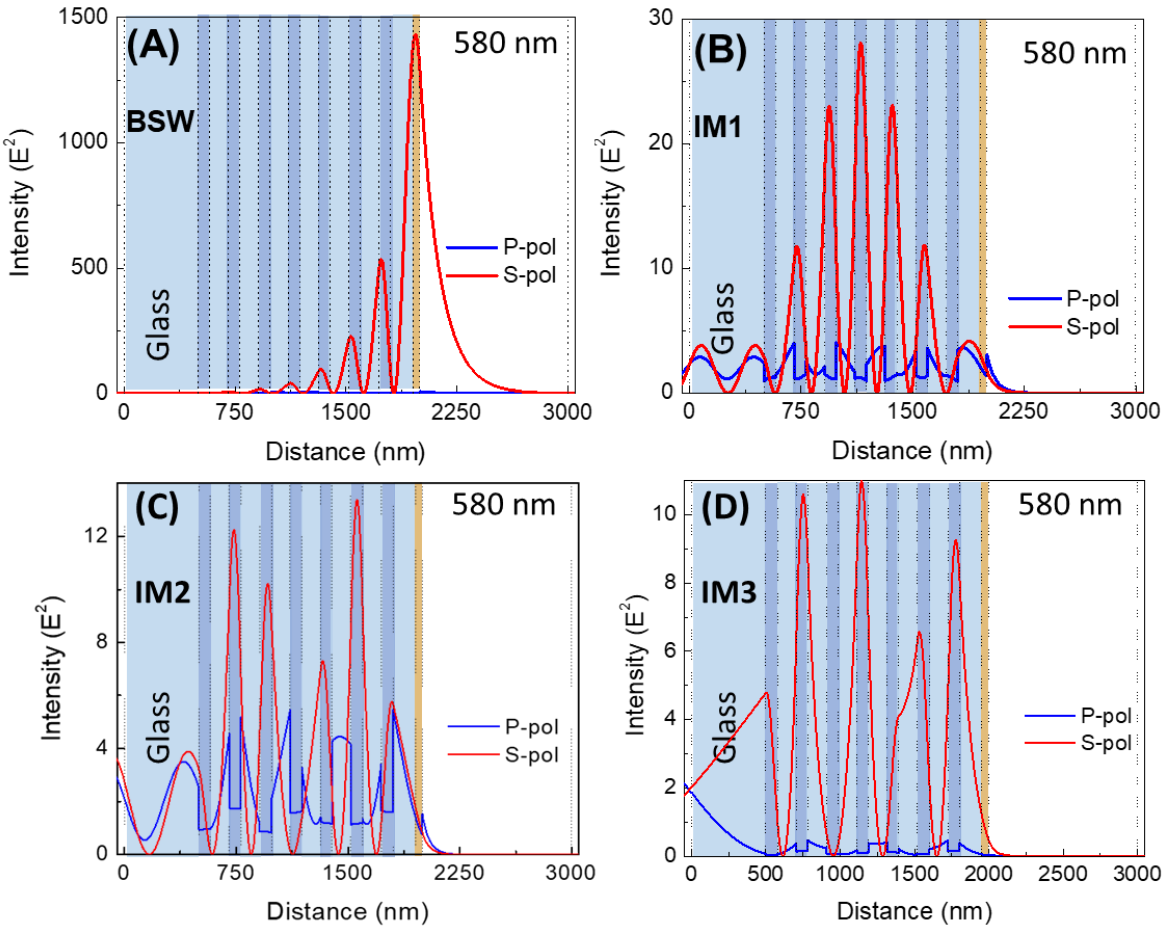

Figure 4. Field intensity ($|E|^2$) distribution for 580 nm incident light. (A) BSW resonance at 44.1 deg, (B) IM1 at 57.8 deg, (C) IM2 at 68.2 deg and (D) IM3 at 85.0 deg. Both S- and P- polarizations are shown.

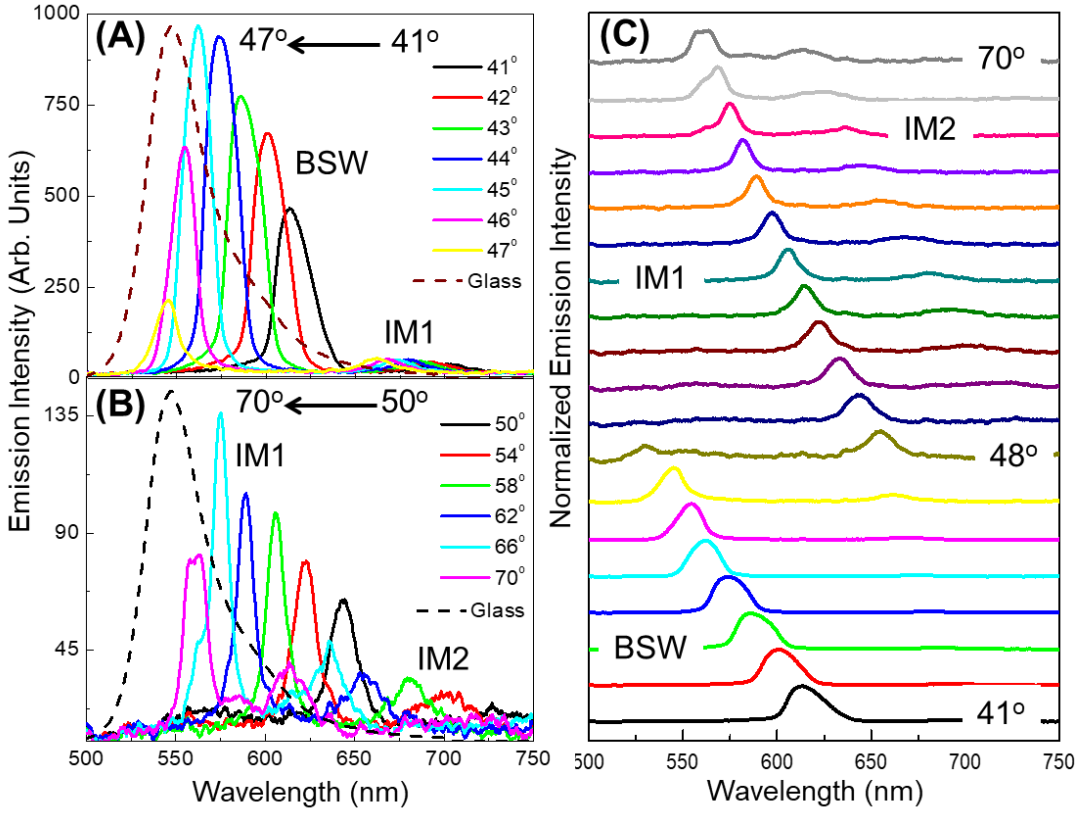

Figure 5. Rh6G, S-polarized emission in the BSW range (A), and in the IM1 range (B). Dashed lines show the intensity normalized Rh6G emission spectrum from glass, which is insensitive to the observation angle. Panel C shows the normalized Rh6G, S-polarized emission in the BSW range and in the ranges for IM1 and IM2. Some selected angles are listed in the panel.

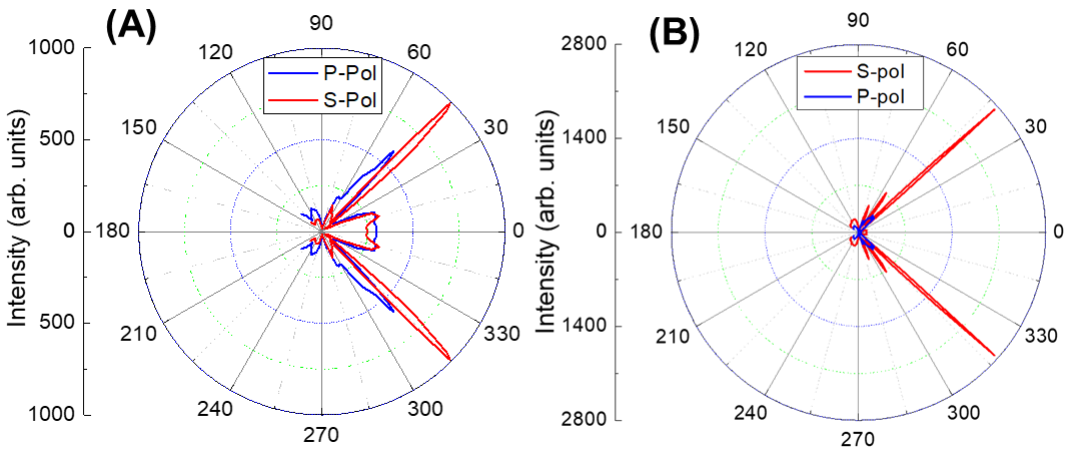

Figure 6. (A), Rh6G and (B) $Ru(bpy)_2(dppz)(PF_6)_2$ angular emission intensity distribution from the 1DPC. RK illumination using 470 nm at 180 degrees.

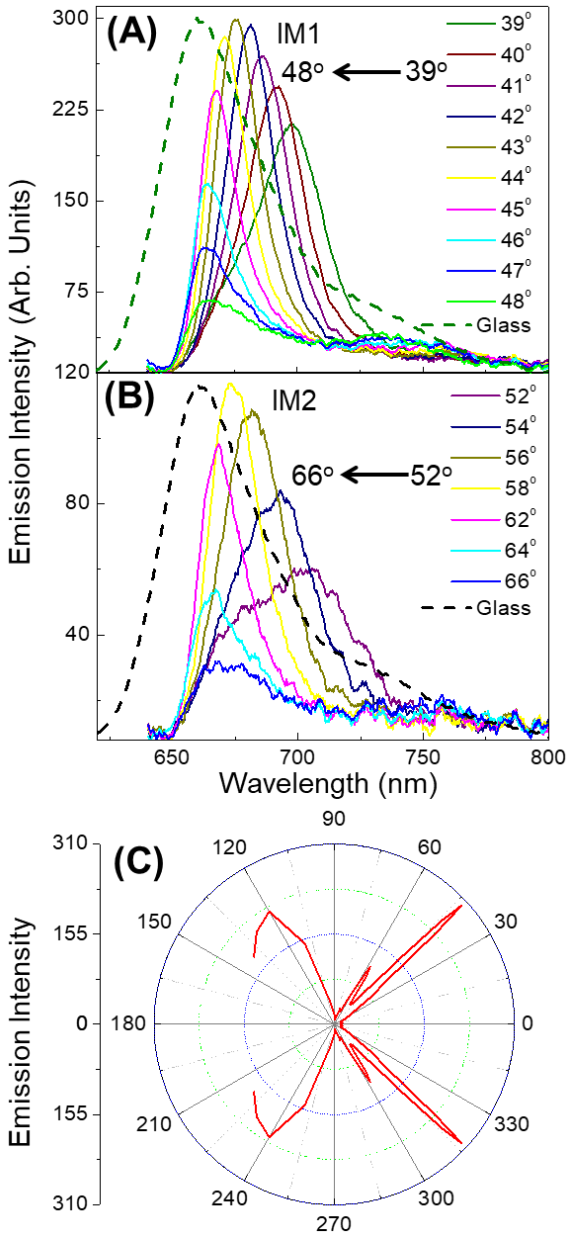

Figure 7. Nile Blue, S-polarized emission in the IM1 range (A), and in the IM2 range (B). Dashed lines show the intensity normalized Nile Blue emission spectrum from glass, which is insensitive to the observation angle. Note the wavelength axis is different from that used in Figure 5. Panel C shows the Nile Blue emission intensity distribution from 1DPC. RK illumination polarized along the Y-axis using 635 nm at 180 degrees.

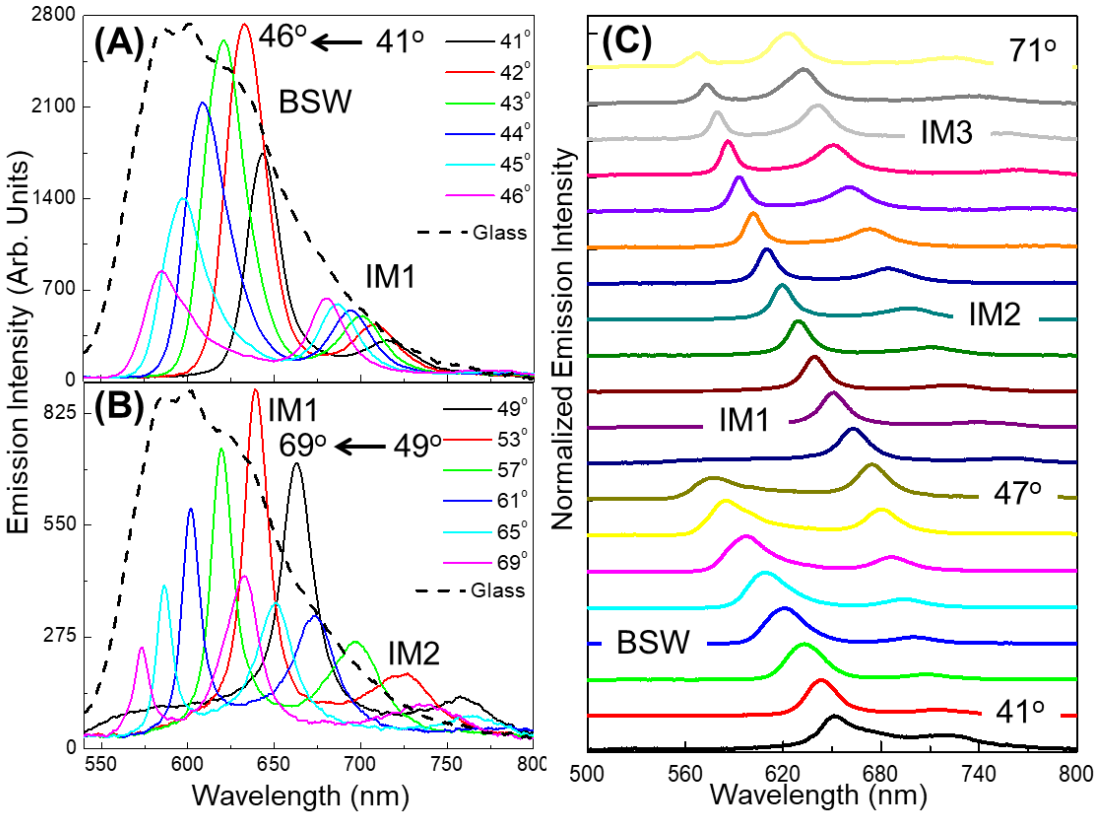

Figure 8. BSW, IM1 and IM2-coupled emission from $Ru(bpy)_2(dppz)(PF_6)_2$ on 1DPC. Dashed lines show the intensity normalized ruthenium complex emission spectrum from glass $\lambda ex = 470$ nm. Panel C shows the corresponding normalized emission in the BSW, IM1, IM2 and IM3 ranges. Some selected angles are labeled in the panel.

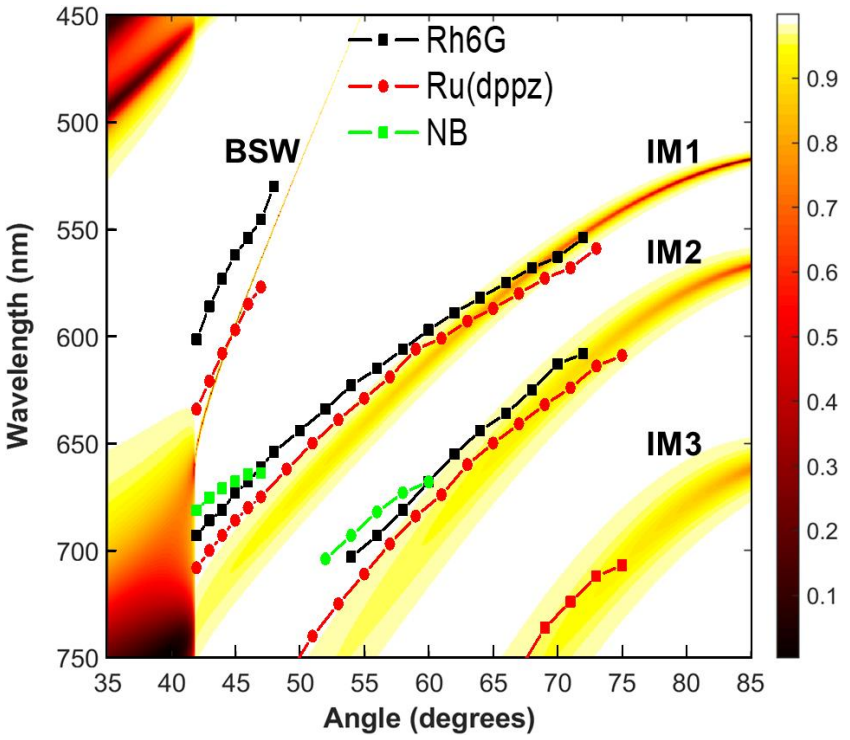

Figure 9. Dispersion diagram for the 1DPC. The figure shows the reflectivity for a range of wavelengths and incidence angles. The dots represent the angle-dependent emission maxima and respective angles.

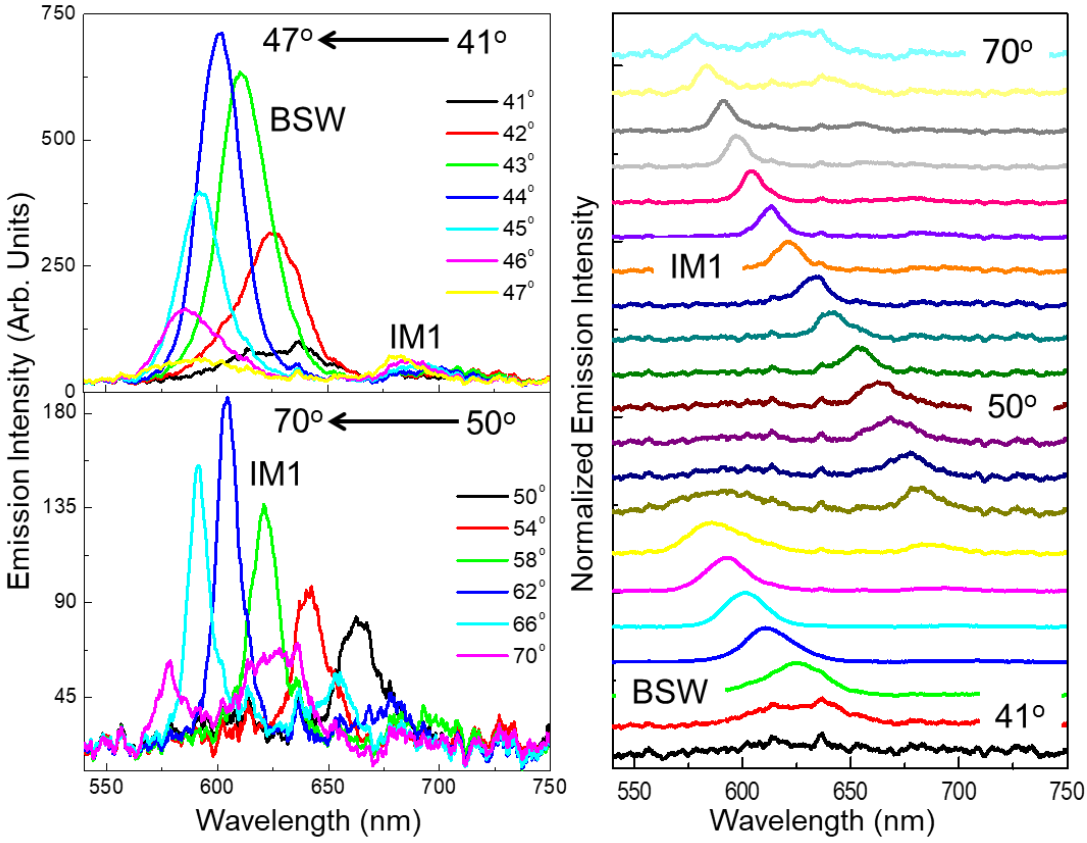

Figure 10. S-polarized emission from a monolayer of RhB-SA on 1DPC in the BSW range, and in the IM1 range. Normalized spectra are shown in the right panel. Only few selected spectra are labeled for clarity.

Figure for TOC Graphic

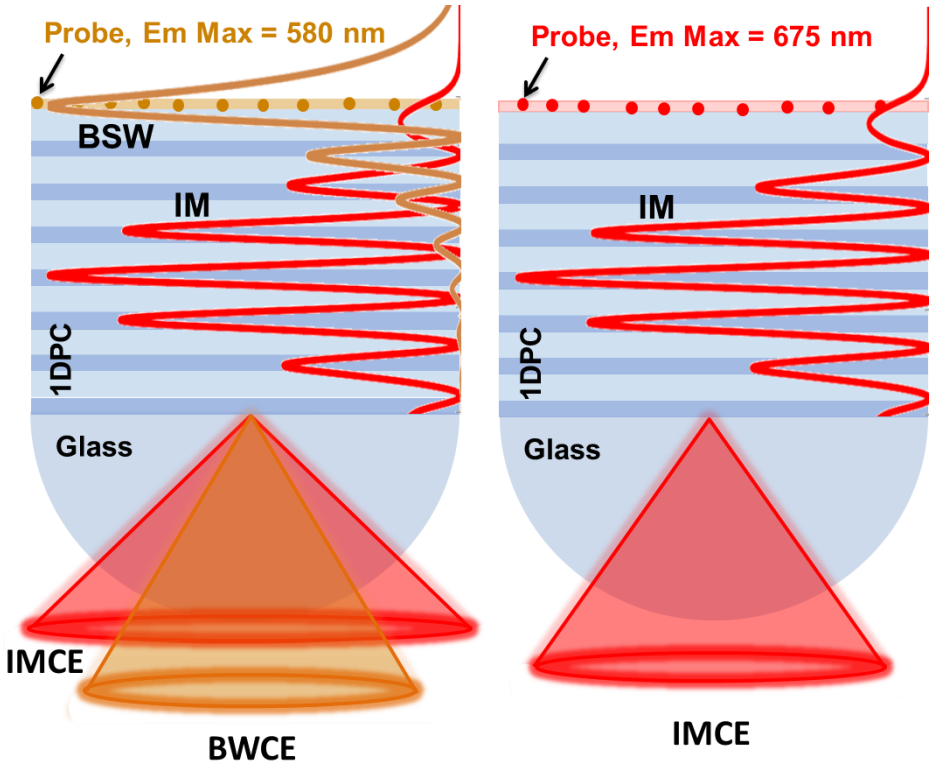

Probe emission wavelength-dependent coupling to optical modes in one-dimensional photonic crystals.

Supplemental information

Fluorophore Coupling to Internal Modes of Bragg Gratings

*Ramachandram Badugu[1], Jieying Mao[1], Douguo Zhang[2], Emiliano Descrovi[3,4], and Joseph R. Lakowicz[1]**

[1]Center for Fluorescence Spectroscopy, Department of Biochemistry and Molecular Biology, University of Maryland School of Medicine, 725 West Lombard Street, Baltimore, MD 21201, USA.

[2]Institute of Photonics, Department of Optics and Optical Engineering, University of Science and Technology of China, Hefei, Anhui, 230026, China

[3]Department of Applied Science and Technology, Polytechnic University of Turin, Corso Daca degli Abruzzi 24, 10129 Turin, Italy

[4]Department of Electronic Systems, Norwegian University of Science and Technology, O.S. Bragstads plass 2b, 7034 Trondheim, Norway

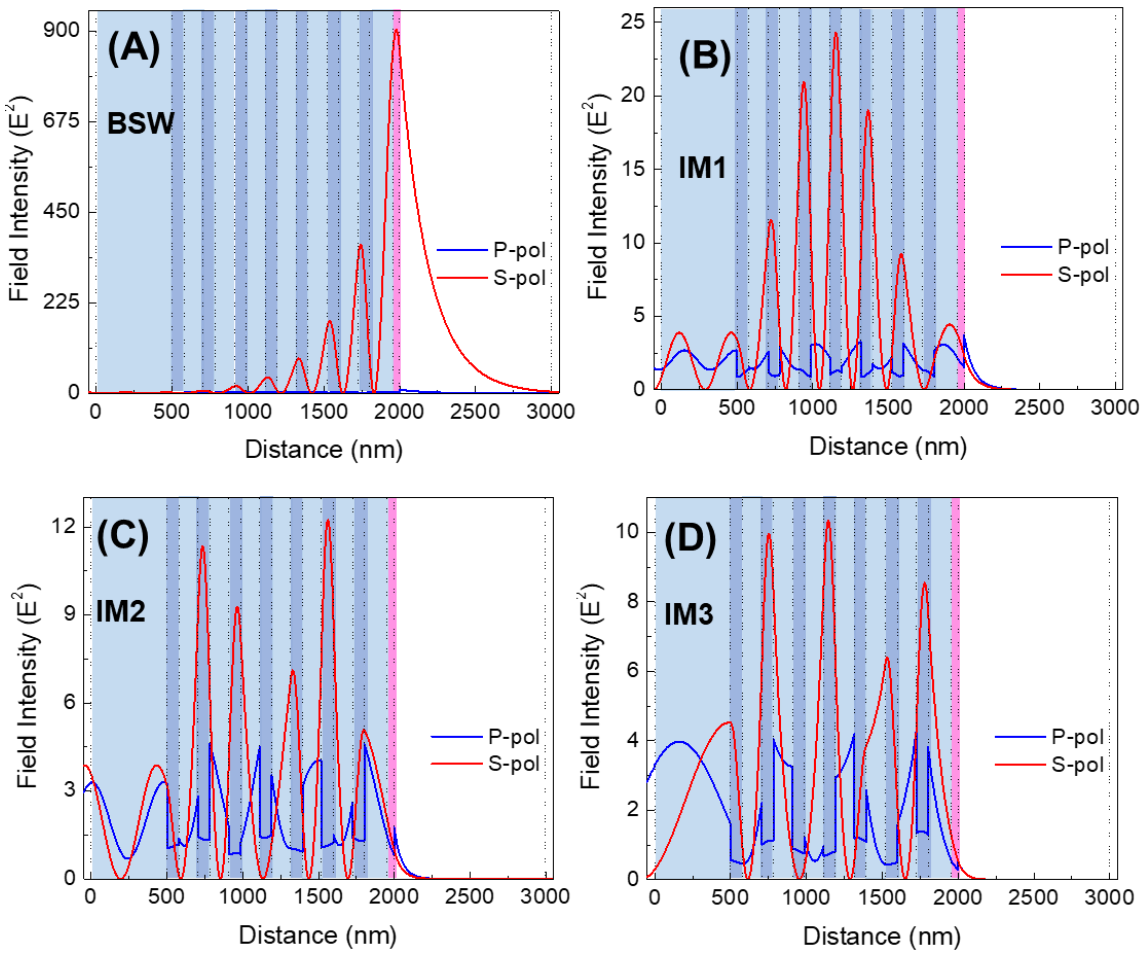

Figure S1. Field intensity ($|E|^2$) distribution for 600 nm incident light. (A) BSW at 42.0 deg. (B) IM1 at 52.9 deg (C) IM2 at 63.3 deg, and (D) IM3 at 85 deg. Both S- and P- polarizations are shown.

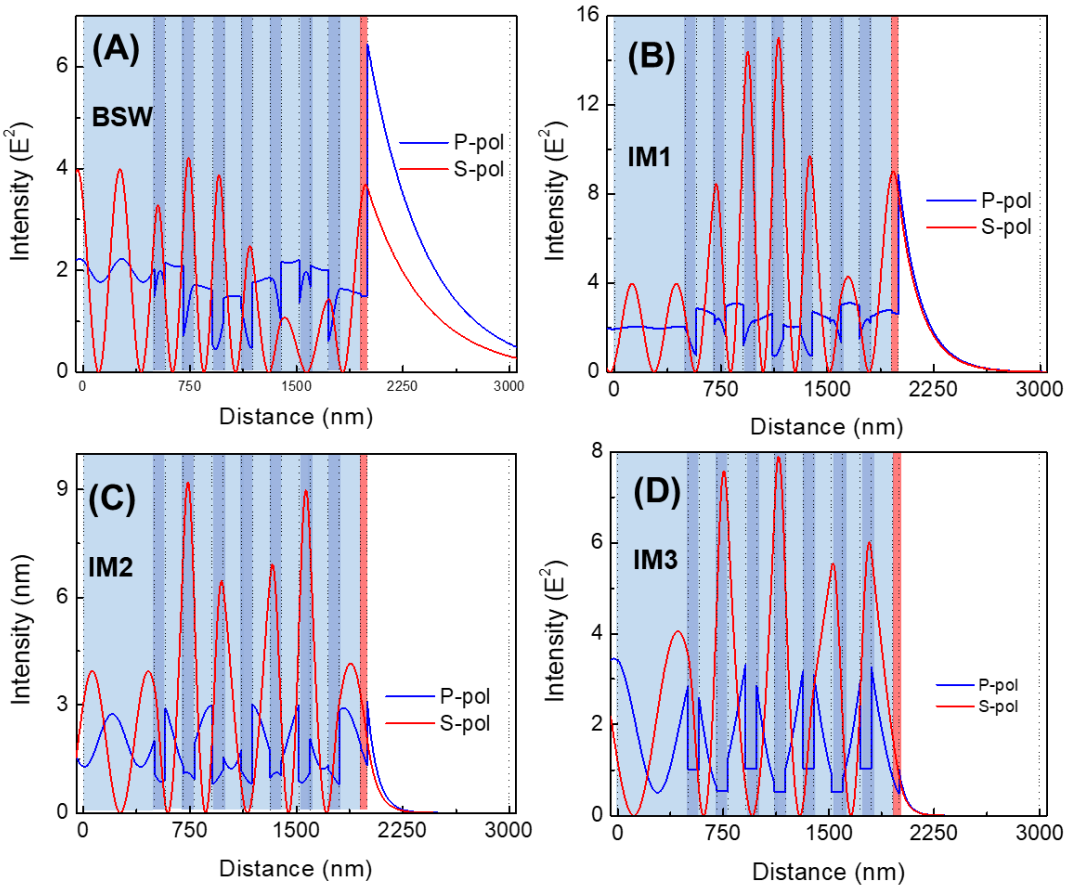

Figure S2. Field intensity ($|E|^2$) distribution for 675 nm incident light. (A) BSW near the critical angle at 41.1 deg. (B) IM1 at 44.1 deg (C) IM2 at 55.7 deg, and (D) IM3 at 68.4 deg. Both S- and P- polarizations are shown.

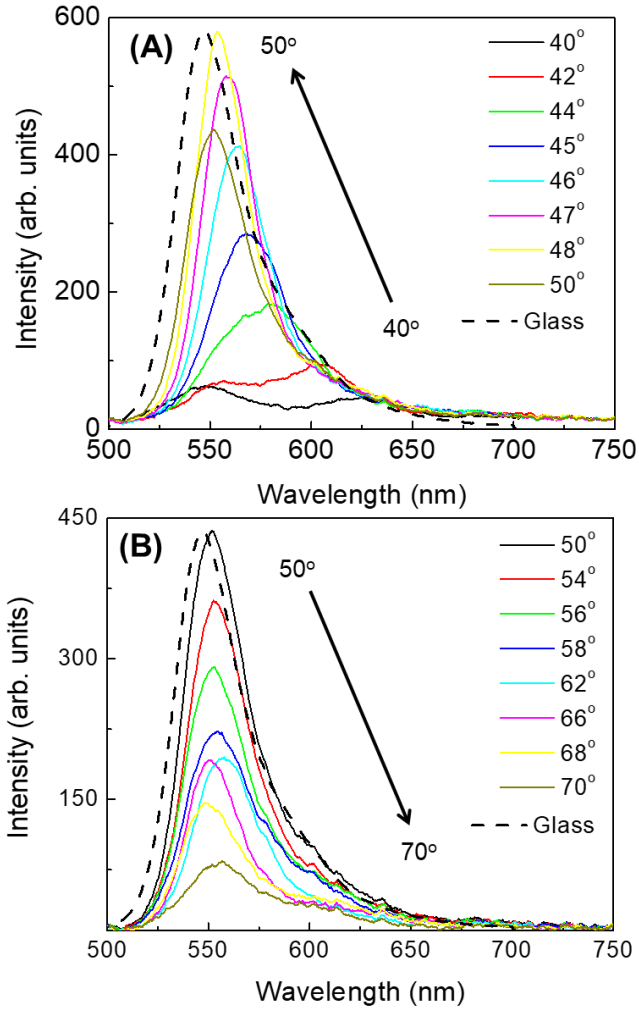

Figure S3. Rh6G, P-polarized emission in the BSW range (A), and in the IM1 range (B). Dashed lines show the intensity normalized Rh6G emission spectrum from glass, which is insensitive to the observation angle.

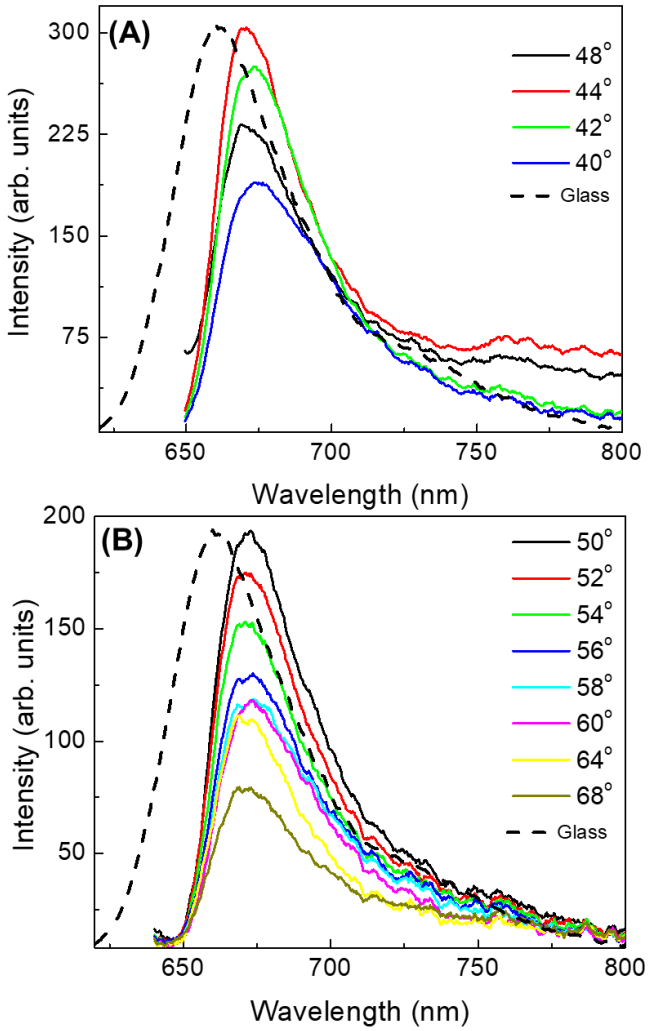

Figure S4. Nile Blue, P-polarized emission in the IM1 range (A), and IM2 range (B). Dashed lines show the intensity normalized Nile Blue emission spectrum from glass, which is insensitive to the observation angle.

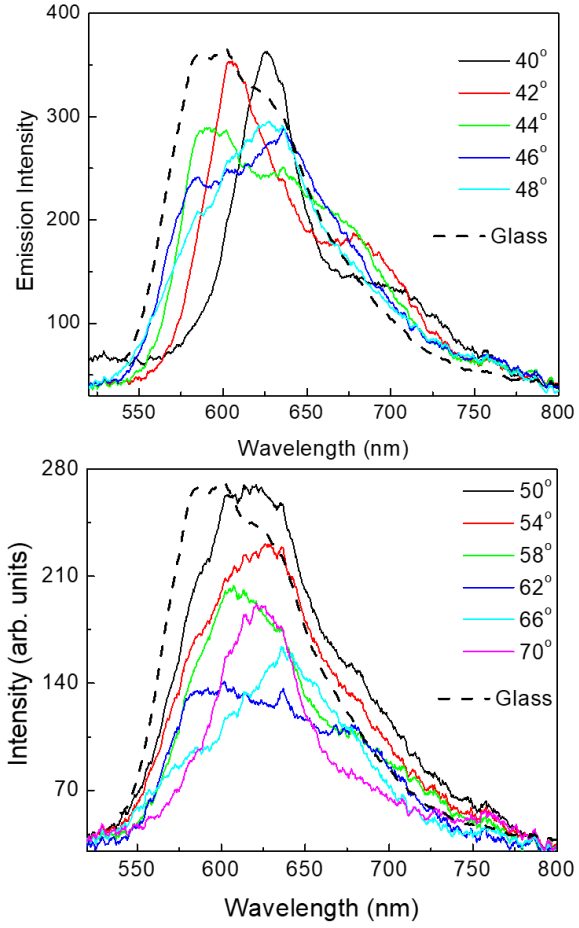

Figure S5. P-polarized coupled emission from $Ru(bpy)_2(dppz)(PF_6)_2$ on 1DPC. Dashed lines show the intensity normalized ruthenium complex emission spectrum from glass $\lambda ex = 470$ nm.

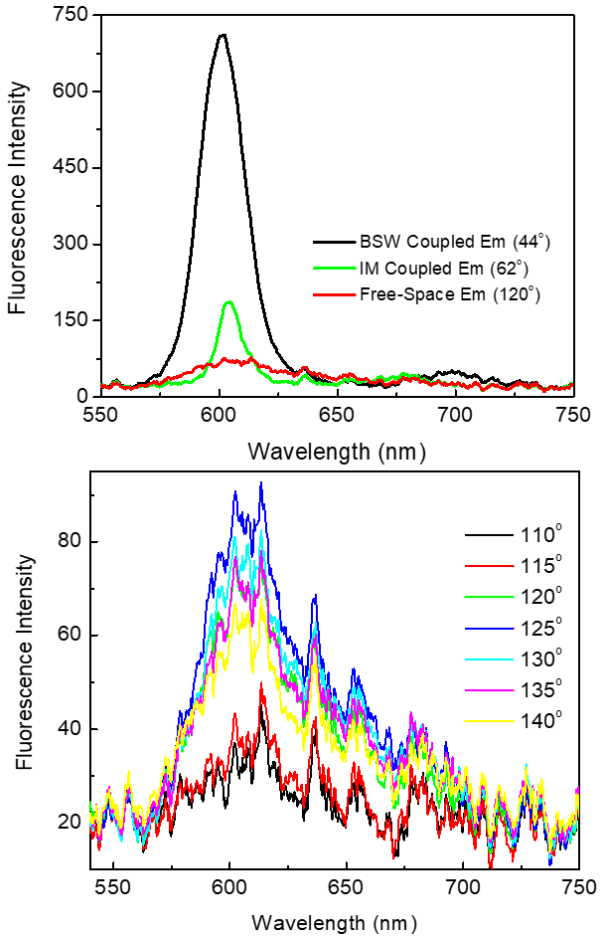

Figure S6. Top, BSW-coupled (at 44 degrees), IM-coupled (at 62 degrees) and free-space emission spectra from a monolayer of RhB-SA on the 1DPC. Bottom, Angle-dependent free-space emission spectra of RhB-SA on 1DPC.